ELSEVIER

Contents lists available at ScienceDirect

Combustion and Flame

journal homepage: www.elsevier.com/locate/combustflame



Confined combustion of polymeric solid materials in microgravity





- ^a Case Western Reserve University, Cleveland, OH 44106, United States
- ^b Universities Space Research Association, NASA Glenn Research Center, Cleveland, OH 44135, United States
- ^c ZIN Technologies, Middleburg Heights, OH 44130, United States

ARTICLE INFO

Article history: Received 15 April 2021 Revised 22 July 2021 Accepted 23 July 2021

Keywords:
Concurrent-flow flame spread
Microgravity combustion
Confined space
Parallel burning samples
Flame wall interactions
Material flammability

ABSTRACT

Microgravity experiments are performed to study the effects of confinement on the burning behavior of polymeric solid materials. Flat, $100 \times 22 \times 1$ mm PMMA samples are burned in concurrent air flow in a small flow duct aboard the International Space Station. Three different burning scenarios are examined, double-sided, single-sided, and parallel samples. In the first two scenarios, single samples are burned on both sides and on one side, respectively. Flat baffles are placed parallel to the sample to confine the available space for combustion. The distance between the baffle and the sample (H) is varied in different tests. In each test, imposed flow is reduced in steps and steady flame spread is achieved at each flow speed until the flame quenches. The results show that at the same confined condition, steady state flame length and spread rate are proportional to flow speed over the range tested. When confinement increases (or H decreases), the flame spread rate and flame length increase first and then decrease. In addition, the quenching flow speed decreases and then increases with decreasing H. These results suggest that the confinement can increase or decrease solid fuel flammability depending on conditions. In the third burning scenario, two PMMA samples are placed parallel to each other separated by a distance H. Twin flames are observed and combustion is confined between the two samples. Among the three tested burning scenarios, twin flames have the largest flame length and burning rate at the same confinement level (H). This is because the thermal interaction between the twin flames enhances the heat feedback to the solid fuel and reduces the relative heat loss to the surrounding flow duct. Comparing single- and double-sided flames with the same baffle-sample distance, the spread rate of a single-sided flame is slightly less than half of that of a double-sided flame. This is due to the halved pyrolysis area exposed to the flame and heat loss on the back side of the sample. Optimal transport of oxygen to the flames also plays a role.

© 2021 The Combustion Institute. Published by Elsevier Inc. All rights reserved.

1. Introduction

Understanding the process of flame spread is crucial for improving fire safety as this process determines the potential time to control and to evacuate from fires. Confinement has been shown to have significant effects on fire characteristics and can potentially increase fire hazards [1]. For example, confinement imposed by external claddings on building facade was recognized to contribute to rapid fire growth in the London Grenfell Tower Fire in 2017. To address this, various technical standards concern burning behaviors of solid materials in different confined environments (e.g., FM 4411 and FM 4880). In one series of tests using FM 4411 test setup, polyurethane was attached to one large panel (1.1 m wide \times 4.9 m high) and burned in a confined space imposed by another parallel panel. The flame was 50% higher (1.8 m versus 1.2 m) when the panel distance reduced from 10 cm to 5 cm [1]. Similar phe-

* Corresponding author.

E-mail address: yating.liao@case.edu (Y.T. Liao).

nomena were found in microgravity. In a previous NASA project, BASS [2,3], 2.2 cm wide and 10 cm long cotton-blend fabrics were burned in air flow in a small flow duct (7.6 \times 7.6 cm cross-section area, 20 cm in length) aboard the International Space Station (ISS). In another project, Saffire [4,5], the same fabric of a significantly larger dimension (41 cm wide \times 94 cm long) was burned in a large flow duct (51 cm \times 46 cm cross-section area, 106 cm in length) in an unmanned space vehicle. The results show that in the same flow and ambient conditions, the sample burns twice as fast in BASS than in Saffire [4,5]. To understand how to interpret data obtained in different test setups and to address the potentially more hazardous fire scenarios in confined spaces, the effect of the confinement on flame spread needs to be carefully evaluated.

The effects of confinement on flame spread were studied in various normal gravity experiments [6–11]. In these experiments, fuel samples were burned in a flow channel [6,12] or next to a structure (e.g., wall [7,8], other burning samples [9–11]). These studies show that for downward flame spread in a confined environment, flame reaches a steady state with constant flame length and spread

rate [6,7,10]. Comas et al. performed downward flame spread over 4 cm wide 26 cm long thin papers both in an open environment and in a channel [6]. The channel has a cross-section area of 4 cm × 4 cm. Inclination angles of the sample (and the channel if used) and ambient oxygen fractions were varied. In all tested conditions, flame traveled slower in the channel than in the open environment. They attributed the slower flame spread rate to lack of lateral entrained air and the friction of walls. Zhu et al. tested downward flame spread over 1 mm thick PMMA slabs next to a parallel wall [7]. One side of the PMMA sample was open to the ambient and the other side was restricted by the wall. The spacing between the sample and the wall was varied. Their results showed that the flame length and flame spread rate increased first and then decreased when the spacing decreased. The maximum burning rate occurred at a medium tested spacing. They concluded that this is due to enhanced radiative heat flux on the fuel surface from the wall at the critical spacing.

In the same experiments of Comas et al. [6], upward flame spread was also tested. When the samples were burned in the flow channel, the flame front spread rate was $\sim 40\%$ higher than that in an open space. They concluded that the increased spread rate is caused by the channeling effect and the enhanced heat transfer to the solid. It was also reported that the flame was significantly stronger than that in the downward flame spread tests and the flame consumed the sample in a very short time (within 2 s). The observation of pyrolysis was seriously impeded by the strong flame.

In downward flame spread, the flame extends upward and covers the burned region of the sample. Only a small bottom portion of the flame transfers heat to the fresh solid fuel. On the contrary, in upward flame spread, the whole flame and the ventilated hot gas products transfer heat to downstream fresh solid fuel. As a consequence, upward flame spread in normal gravity usually has a longer flame length and a higher spread rate compared to the downward flame spread. Furthermore, the induced buoyancy flow is strongly correlated to the concurrent-flow flame size and the upward flame spread is commonly acknowledged as an accelerating process [13]. These factors introduce challenges for fundamental investigations on concurrent-flow flame spread in normal gravity.

In microgravity, the confounding factors of buoyancy flow are eliminated. Instead of being categorized as upward and downward, flame spread is considered concurrent or opposed depending on the relative direction of the flame spread to the flow. Note that downward flame spread in normal gravity is also considered as opposed-flow as the buoyancy flow goes up and upward flame spread as concurrent-flow. Wang et al. examined the effect of confinement on opposed-flow flame spread using CAS (Chinese Academy of Sciences) 3.6 s drop tower [14]. In their experiments, thin papers were burned in flow ducts of various duct heights (ranging from 1.5 cm to 5 cm). When the duct height decreased, the flame length and spread rate increased first and then decreased. They also conducted complementary numerical simulations. The modeling results showed that the stronger flame at medium duct height was due to local flow acceleration caused by combustion thermal expansion. This flow acceleration is suspected to have an even more profound effect on solid burning behaviors in concurrent flows than in opposed flows as the flame-solid coupling is stronger.

Olson conducted experiments of concurrent-flow flame spread over three parallel cheesecloth sheets using NASA's 5.18 s drop tower [15]. The inter-sample distance varied between 1.27 cm and 3.81 cm. The three samples were ignited simultaneously, and the edge view of flame spread was recorded. Flame spread of a single sample was also tested for comparisons. When the sample separation distance is large (3.18 cm), the parallel samples have a larger flame spread rate compared to the single sample. This was

attributed to the radiative heat transfer between adjacent burning samples. When the separation distance is small (1.27 cm), the burning intensity of parallel samples is lower than that of a single sample. This is due to insufficient oxygen supply to the combustion zone.

Other than Olson's work, to the authors' best knowledge, there is no microgravity experiment that explicitly investigates the effects of confinement on concurrent-flow flame spread. Olson's experiments focused on thin cellulose samples and short-time quasisteady flame behaviors (likely due to the limitation in test duration in a drop tower). To achieve a more complete understanding of how flame spreads in a confined space, more investigations on various confined conditions are needed.

In this study (referred to as Confined Combustion), concurrentflow flame spread was investigated using the BASS flow duct aboard the ISS [2,3]. The long test duration allows the observation of different flame development (accelerating flame spread, steady state, and extinction) when subjected to different confinements. The long microgravity duration also allows thicker samples to be tested. In Confined Combustion, thin cotton-blend fabrics and 1mm-thick cast PMMA slabs were tested. Results of the thin fabric were published in a separate paper [16]. In this work, results of PMMA are presented. Three different burning scenarios were considered: symmetric double-sided burning, single-sided burning, and burning of parallel samples. Effects of confinement in each scenario are investigated and compared. Imposed flow speed is also varied to investigate its interplay with the confinement. The aim is to provide a comprehensive understanding on how polymeric materials interact with its surrounding structures during combustion.

PMMA is commonly used in aerospace and earth applications, and as a solid fuel calibration specimen, hence is frequently tested in normal gravity [7,8,17] and microgravity experiments [5,18–20]. The previous experiments focused on burning behaviors in different flow speeds [19,20], flow direction [7,8,20], oxygen concentration [19,20], and sample shapes [5,18,20]. The results of Confined Combustion can be potentially compared to results from other experiments. The results can also potentially provide guidance for product design and development of fire safety codes.

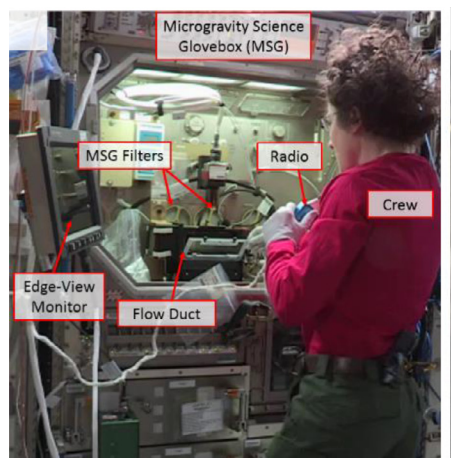
2. Microgravity experiment

2.1. Experimental apparatus

Confined Combustion, was developed upon a previous NASA project, Burning and Suppression of Solids - BASS [2,3]. Burning experiments were conducted inside a small flow duct contained in the Microgravity Science Glovebox (MSG) aboard the ISS, as shown in Fig. 1. The flow duct is 20 cm long and has a cross-section area of 7.6 cm \times 7.6 cm. A fan section is integrated at the inlet of the flow duct and is capable of providing a maximum flow speed of 55 cm/s [21]. The flow duct was refurbished and updated on the ground prior to being sent back to the ISS. Modifications were made to accommodate a new sample/baffle assembly for achieving different effective flow confinement for this project.

The flow duct features a front and a top window, allowing observation of the burning event. A high-resolution video camera was used to record the burning process from the edge view (parallel to the sample) through the top window. During the experimental operation, the camera was set to auto adjust for white balance, exposure, and digital gain. The spatial resolution and the frame rate of the video recording are 12.5 pixels/mm (or 0.08 mm/pixel) and 24 frames per second (or \sim 42 ms/frame) respectively.

In all experiments, the ambient conditions in the MSG were maintained at 1.0 atm and \sim 22% oxygen molar fraction (i.e., the ISS conditions). The oxygen molar fraction X_{O_2} was monitored by



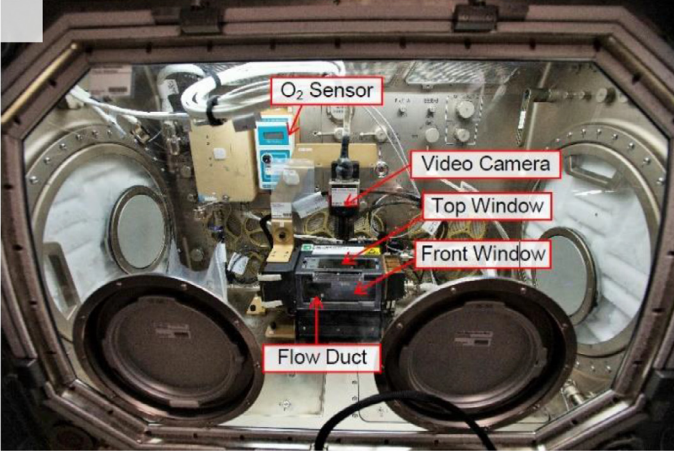
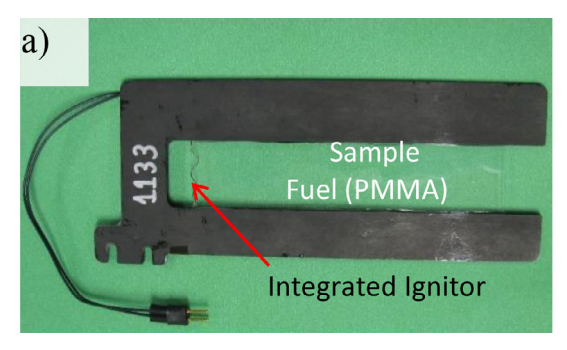


Fig. 1. Experimental setup in the Microgravity Science Glovebox aboard the International Space Station. A sealing front window for containment and a cloth light cover are installed over the MSG work volume before each test run. a) ISS crew member sets up and performs each test while in real time space to ground communication with the science team in the Glenn Research Center ISS Payload Operations Center (GIPOC). b) Close-up view of the experimental setup.



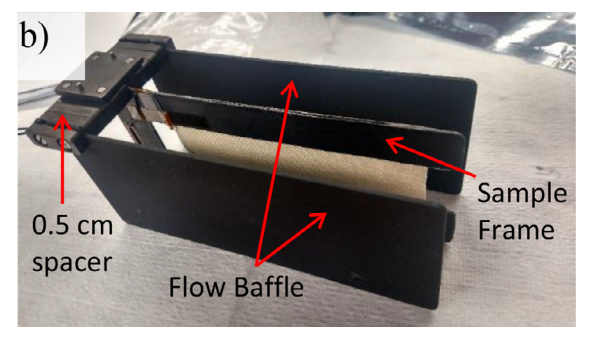


Fig. 2. a) Sample frame with fuel and igniter. b) Assembly of the sample/baffle carrier, sample frame, and two parallel flow baffles.

an O_2 sensor (Quantek model 201 accuracy +/-2% of reading) inside the MSG (Fig. 1). The daily oxygen variation was measured to be between 21.3% and 22.9%.

During each operation, real-time space to ground communication and live video downlink were established between ISS crew and the science team in the NASA Glenn Research Center ISS Payload Operations Center (GIPOC). The experiments were instructed and monitored by the science team and were operated by the ISS crew.

2.2. Sample-baffle assembly

Two sample materials were tested in Confined Combustion: thin cotton-blend fabric and 1mm-think PMMA slab. Results for the thin fabric were reported in a previous paper [16] and this work focuses on the results for the PMMA samples. The samples are made of uncoated clear CLAREX® cast acrylic sheet. Each sample is sandwiched by thin black anodized stainless-steel frames (as shown in Fig. 2a) leaving the burning area exposed. The sample frame is 13.8 cm long and 6.1 cm wide and the exposed sample area is 10 cm long and 2.2 cm wide. To ignite the sample, a 29-AWG Kanthal sawtooth-shaped electric wire (\sim 1 Ω , powered at 3.7A) is wrapped on the sample at the upstream leading edge.

Flow baffles (made of black anodized 6061 aluminum alloy, shown in Fig. 2b) are used to impose flow confinement on the concurrent-flow flame during the burning process of the sample. Baffles and sample frames are positioned in the flow duct using a newly developed baffle/sample mounting system (Fig. 2b). The system consists of a series of 0.5 cm spacer blocks and is attached to the flow duct top window using a magnet. Flow baffles and sample frame can be inserted into any positions between the spacer

blocks. This setup allows a variety of sample configurations. In this work, three different burning scenarios are tested (Fig. 3): double-sided flame, single-sided flame, and twin flames.

In Fig. 3a, the sample is positioned in the center of two baffles. After ignition, flames are observed on both sides of the samples. Hence, this burning scenario is referred to as double-sided flame. Confinement of the combustion is controlled through the interbaffle distance 2H. In Fig. 3b, one baffle (referred to as quenching baffle) is placed one-spacer away (0.5 cm) on the back side of the sample and another baffle is placed at distance H from the sample surface. The back quenching baffle restricts the flow and prohibits the flame on the back side of the sample. As a result, the sample burns one-sided. In Fig. 3c, two PMMA slabs are positioned in parallel with a separation distance H. Quenching baffles are placed one spacer away on the back of both samples to ensure one-sided burning for each sample. Twin flames, one from each sample, are observed in this burning scenario.

In all three configurations, the sample frame is positioned in the center of flow duct. In this work, the confinement of the combustion event is characterized by the baffle distance H (see Fig. 3). The effects of confinement on each of the burning scenarios are discussed and compared.

2.3. Test matrix

In addition to sample configurations and the baffle distance, the imposed flow speed is also a varying parameter. In the beginning of all tests, an initial constant flow speed was imposed. After the flow stabilized, the ignitor was powered at \sim 3.7 A and lasted until a visible flame was observed (7 \sim 20 s). After ignition, the flow speed was decreased in steps until the flame fails to spread down-

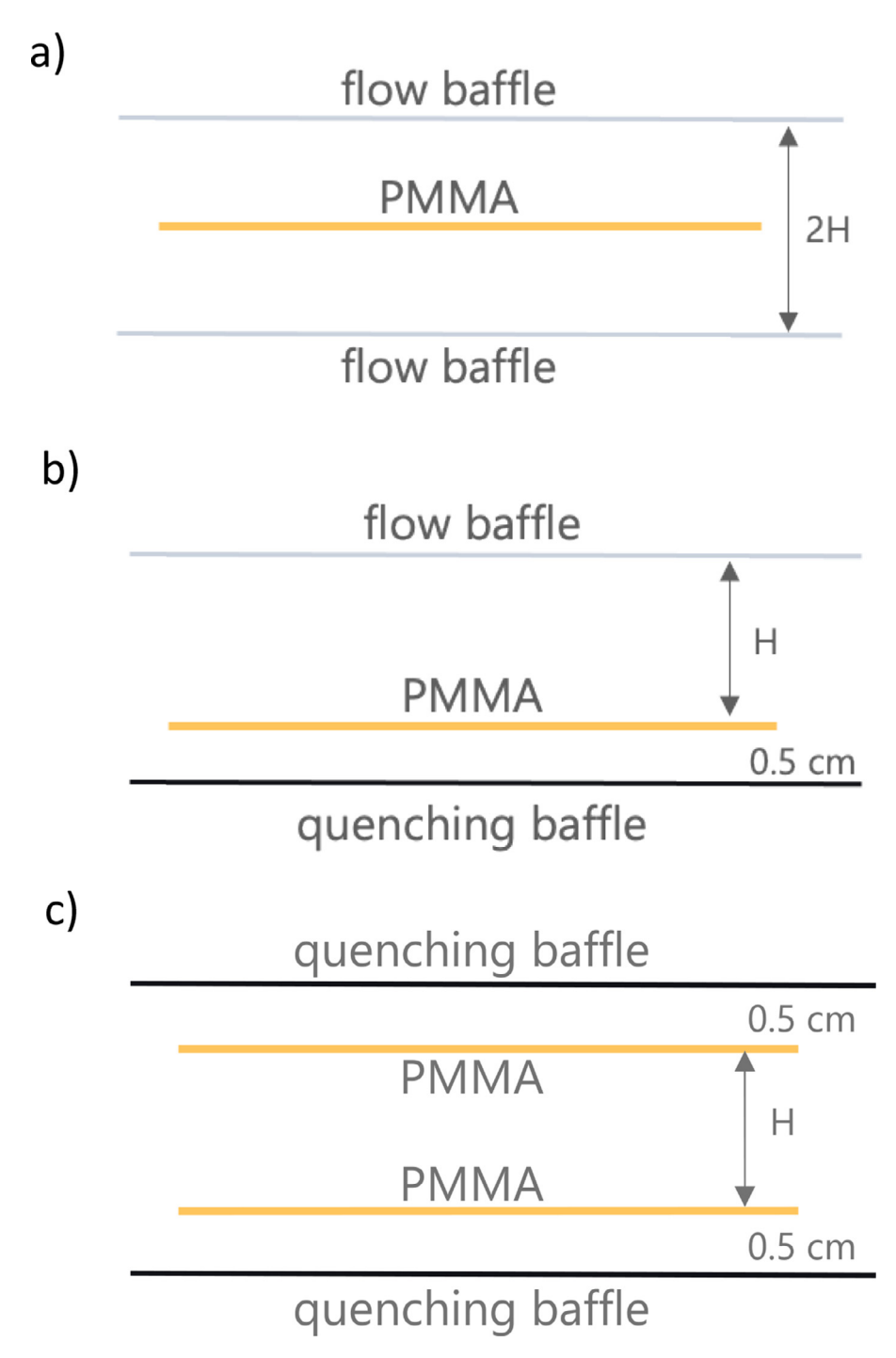


Fig. 3. Sketch of sample/baffle configurations: a) double-sided flame, b) single-sided flame, and c) twin flames. Not to scale.

stream. After each flow reduction, flow speed was maintained for at least 200 s, allowing the flame to adjust to the new flow conditions. This procedure (documented in Table 1) is similar to that in BASS [3] and allows multiple flow speeds to be tested in one burn. Figure 4 summarizes the conditions for which steady flames were observed in this work.

3. Transient flame development

3.1. Single-sided flames

The development process of single-sided flames is demonstrated using a representative case with $H=2.5\,$ cm, shown in

Fig. 5. Shortly after the ignitor is energized, a gaseous flame is observed at the upstream leading edge of the sample. The flame is very bright and turbulent under the initial flow speed (~ 11 cm/s). Flame is sooty and exhibits periodic sparks near the downstream front. These sparks are suspected to be due to fuel vapor-jetting [18]. During the burning process, solid PMMA melted before it vaporized. Due to the absence of gravity, the melted PMMA stayed in place on the sample surface and did not drip. As a result, gaseous pyrolysate is sometimes trapped by the melted PMMA and forms bubbles on the heated sample surface. When these bubbles burst, fuel vapor is released in jets and penetrates the flame zone, causing disturbance of the flame shape. As the flow speed decreases, the flame becomes dimmer and more laminar. This vapor jetting

Table 1Test matrix of imposed flow speed and confinement level.

Burning Scenario	Baffle distance (H: cm)	Imposed Flow (cm/s)
Single-Sided	1.0	$7.3^{\text{a}} \rightarrow 6.2 \rightarrow 5.2 \rightarrow 4.7 \rightarrow 3.9$
-	1.5	$11^a \rightarrow 7.3 \rightarrow 5.1 \rightarrow 3.9 \rightarrow 2.5 \rightarrow 2.0^b$
	2.0	$11^a \rightarrow 7.3 \rightarrow 5.3 \rightarrow 3.9 \rightarrow 2.5 \rightarrow 1.9^b$
	2.5	$11^a {\rightarrow} 7.3 {\rightarrow} 5.1 {\rightarrow} 3.9 {\rightarrow} 2.5 {\rightarrow} 2.2^b$
	3.8 (No baffle)	$11^a {\rightarrow} 7.3 {\rightarrow} 5.2 {\rightarrow} 3.9 {\rightarrow}\ 2.5 {\rightarrow} 2.2^b$
Double-Sided	0.5	$6.1^a\!\!\to\!\!7.0\!\!\to\!\!7.6\!\!\to\!\!10.4\!\!\to\!\!13.3\!\!\to\!\!16.5\!\!\to\!\!7.4^b$
	1.0	$7.5^{a} \rightarrow 5.2 \rightarrow 3.9 \rightarrow 2.4 \rightarrow 3.9 \rightarrow 3.0^{b}$
	1.5	$5.2^{a} \rightarrow 2.5 \rightarrow 2.0 \rightarrow 1.7^{b}$
	2.0	$7.7^{a} \rightarrow 1.8 \rightarrow 1.6^{c}$
	2.5	$5.2^{a} \rightarrow 1.8 \rightarrow 1.7^{b}$
Twin Flames	1	$7.3^{a} \rightarrow 5.2 \rightarrow 3.9 \rightarrow 2.6^{b}$
	1.5 ^d	$7.3^{a} \rightarrow 8.5 \rightarrow 10.3 \rightarrow 16.4 \rightarrow 7.3 \rightarrow 6 \rightarrow 4.7 \rightarrow 16.4^{c}$

- ^a Initial flow speed for ignition.
- ^b Flame quenched within 10 s at this flow speed.
- ^c Flame sustained and consumed the sample at this flow speed.
- ^d Flame from the first sample did not ignite the second sample.

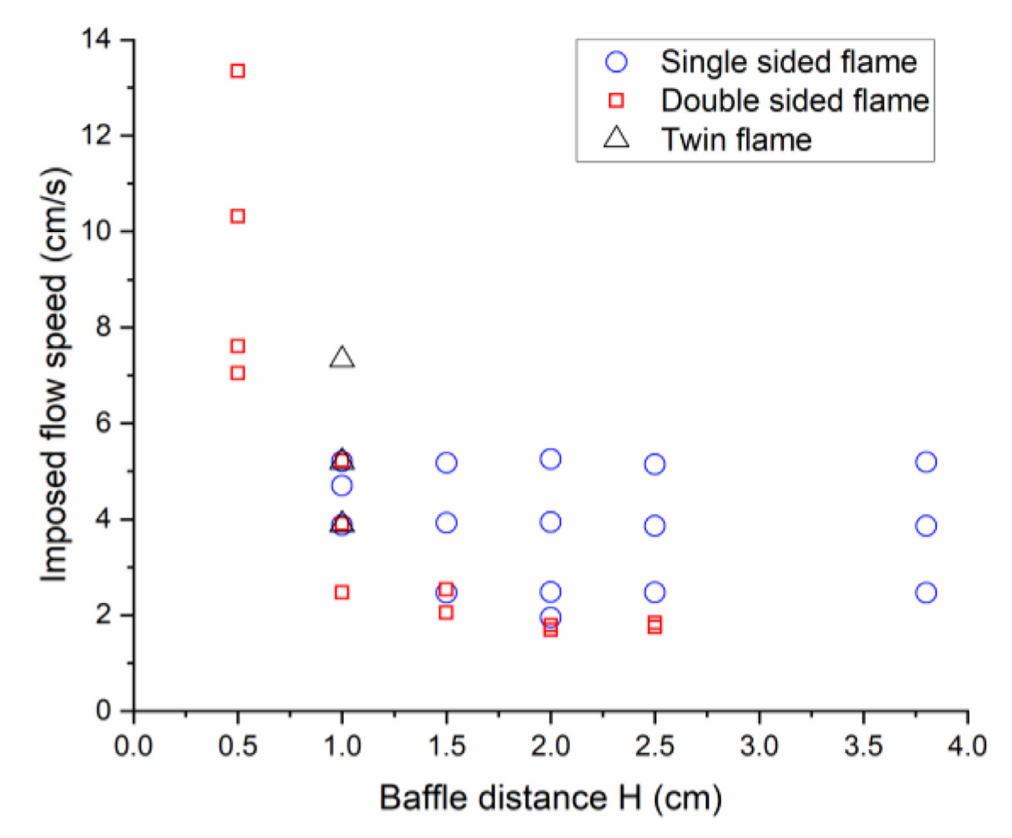


Fig. 4. Test points where steady flames are obtained for PMMA samples in Confined Combustion.

phenomenon is mitigated as well. Notice that at decreased flow speeds (e.g., $U_0 = 5.1 \text{ cm/s}$), the flame turns blue, suggesting less soot formation and lower flame temperature. Smaller flame length and spread rate are also observed at lower flow speeds. For this representative case, when the imposed flow speed is reduced to below 2.5 cm/s, flame gradually decays and eventually quenches.

The video image frames were analyzed using an inhouse code using Matlab Image Analysis Toolbox, which transforms the images into binary, then extracts the flame boundary, and tracks the flame location over time. Details of the code and the flame location tracking methodology can be found in [16].

Figure 6 shows the locations of the flame front and flame base (most downstream and most upstream points of the flame respectively), flame length (difference between the flame base and flame front locations), and the imposed flow speed during the operation.

The plot shows that the flame was able to adjust and reach the steady state at three tested imposed flows (5.1, 3.9, and 2.5 cm/s respectively, marked by the shaded areas in Fig. 6). For each tested flow rate, linear least-squares curve fit is applied to the flame front and flame base data. Slopes of the fitted lines are used to calculate the flame spread rate. Average flame length is also deduced for each steady spread stage.

In a previous study, Zhu et al. conducted experiments to investigate upward flame spread over PMMA slabs in normal gravity [8]. In their work, 1 mm thick, 5 cm wide, and 20 cm long PMMAs were burned next to a wall. For a confined condition similar to that in Fig. 6 (sample-wall distance = 2.5 cm), the flame was observed to continually accelerate throughout the burning process. This accelerating flame spread was due to the increasing buoyancy flow induced by the flame during the burning process and was

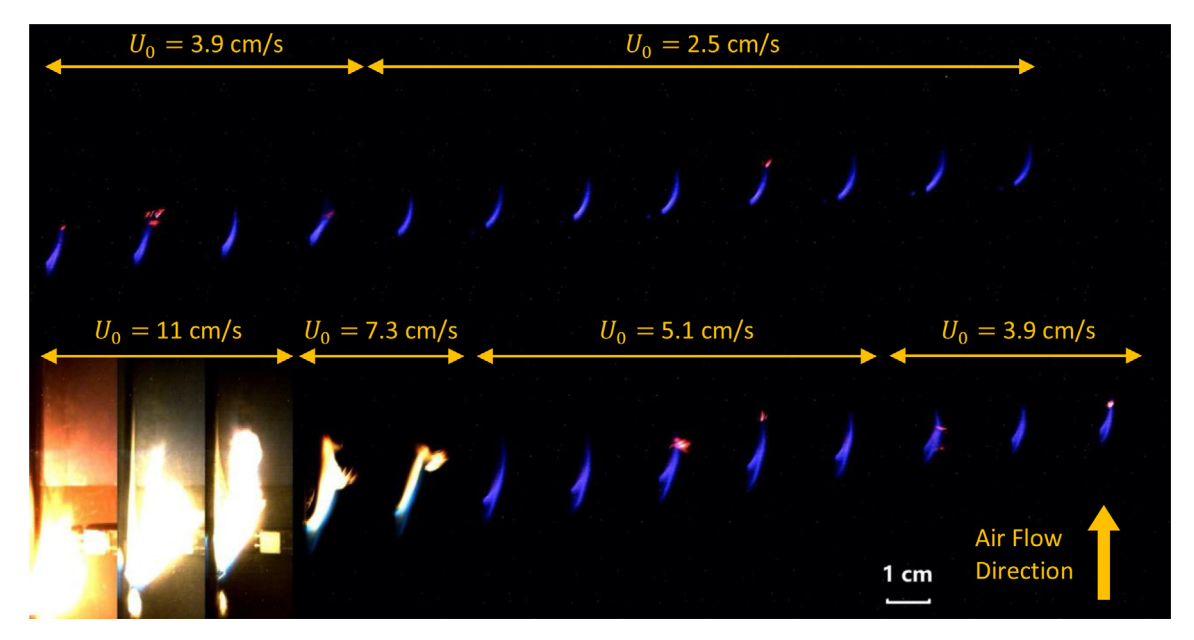


Fig. 5. Transient flame spread process of the single-sided flame (H = 2.5 cm). Ignition is on the lower left and images are 50 s apart, left to right, bottom row to top row.

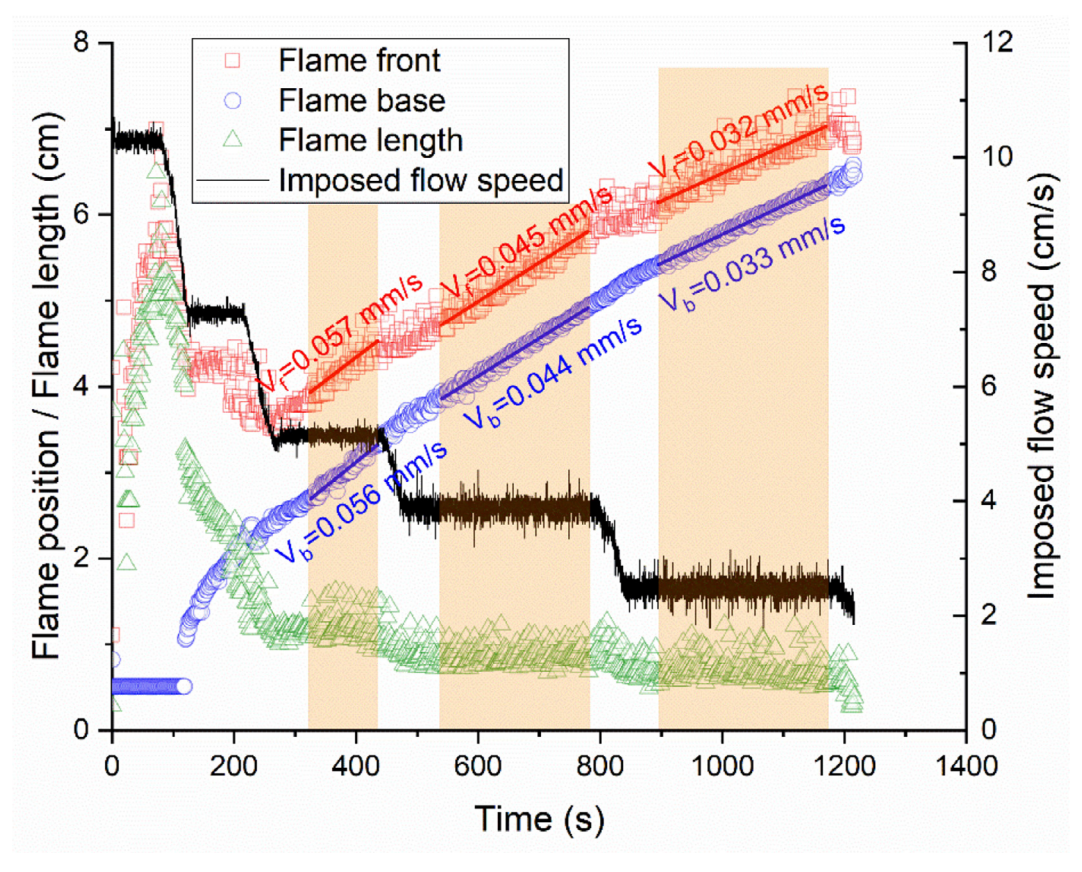


Fig. 6. Flame position and flame length evolution after ignition (single-sided flame with H = 2.5 cm).

fundemethally different from the steady spread observed in microgravity. When the flame spread to the end of the 20 cm long sample, the flame spread rate (>3 mm/s) was recorded two order of magnitude larger than those obtained in microgravity in this work. The buoyancy flow and the chimney effect signifacntly increase the flame spread rate in normal gravity.

3.2. Double-sided flames

The burning process of the double-sided flame is shown in Fig. 7 using a representative case with the inter-baffle distance 2H = 3.0 cm. With this symmetric baffle setup, gaseous flames are observed on both sides of the sample after ignition, similar to that

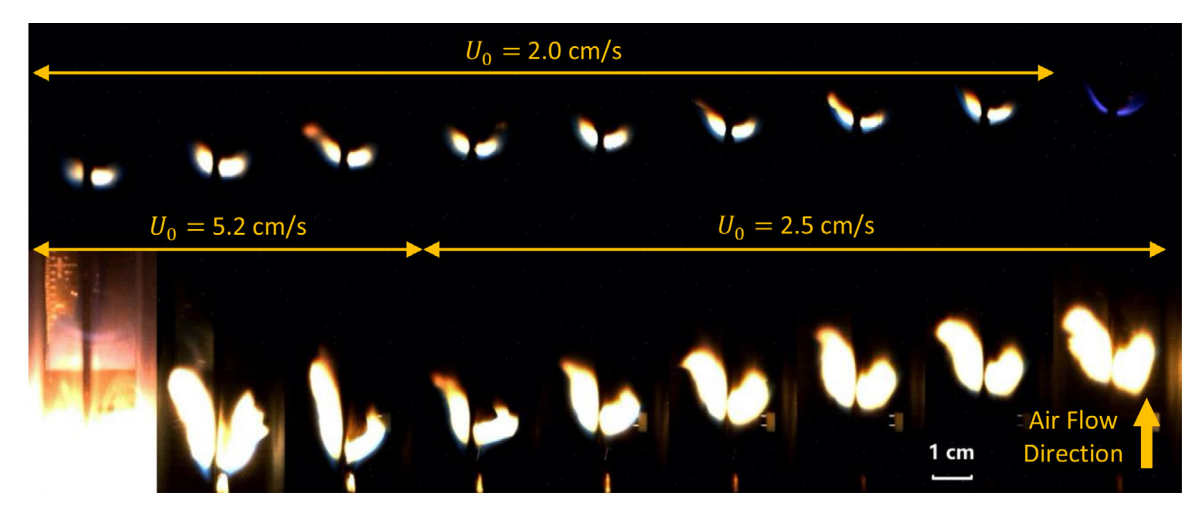


Fig. 7. Transient flame growth of the double-sided flame (H = 1.5 cm). Ignition is on the lower left and images are 33 s apart, left to right, bottom row to top row.

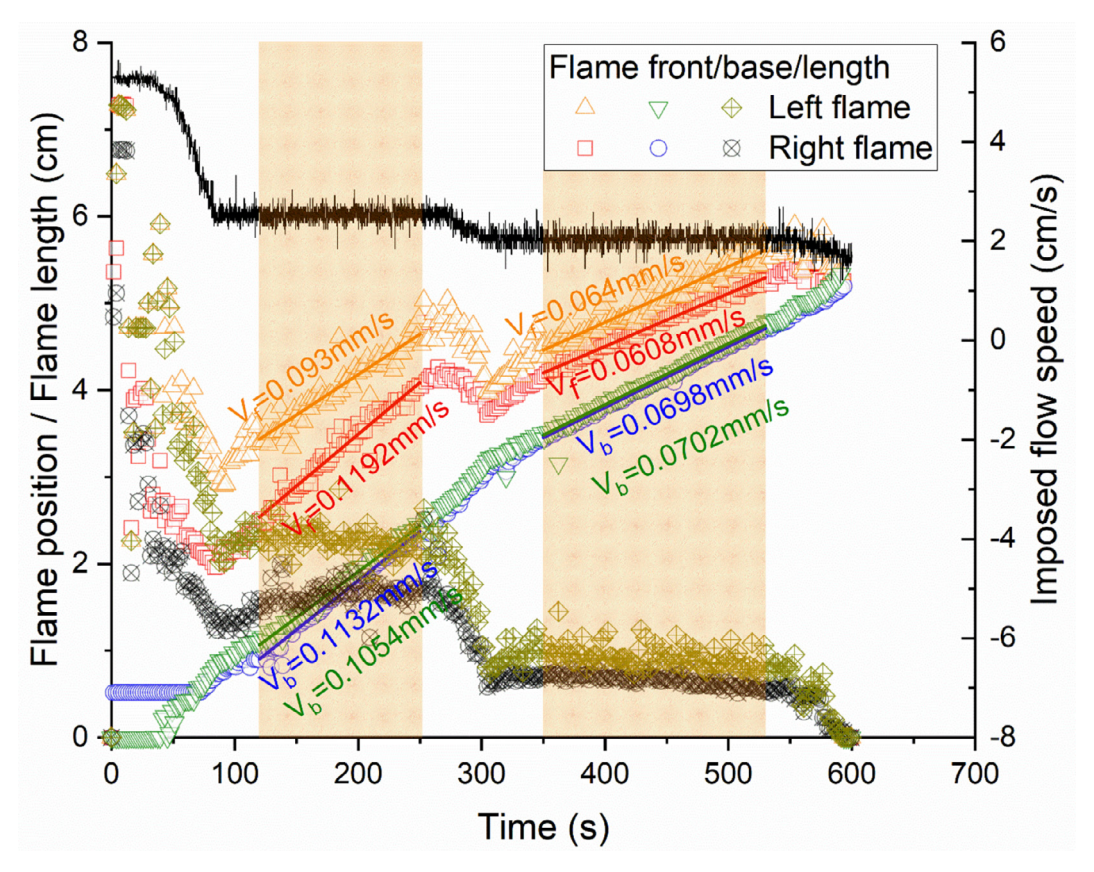


Fig. 8. Flame position and flame length evolution after ignition (double-sided flame with H = 1.5 cm).

reported in [16]. Similar to single-sided flames, as the flow speed reduces, the flame length decreases. In this representative case, when the imposed flow speed decreases to below 2.0 cm/s, flame turns blue and becomes dimmer. Eventually, the flames on both sides of the sample quench and fail to spread further downstream.

Figure 8 shows the front and base locations and the lengths of the flames on both sides of the sample. Steady double-sided flames were observed at imposed flow speeds of 2.5 cm/s and 2.0 cm/s. Notice that in this representative test, the flame on the left side is $\sim 37.6\%$ longer and closer to the sample surface compared to the flame on the right side. This is likely due to sample surface distortion during the test. When being subject to the heat from the flame (or the ignitor), the fuel sample expands and bends slightly

toward one side, leading to an asymmetric geometry and flow conditions. This asymmetric flame shape is not consistent between different tests. A stronger flame can occur on either side of the sample. Nevertheless, in all tests, the flame base spread rates deduced from left and right flames are similar (< 7% difference). When comparing the flame spread rates between different confinement and flow conditions, averaged values between the left and right flames are used.

3.3. Twin flames

The flame spread process of the twin flames is shown in Figs. 9 and 10. In this test, two parallel samples were positioned

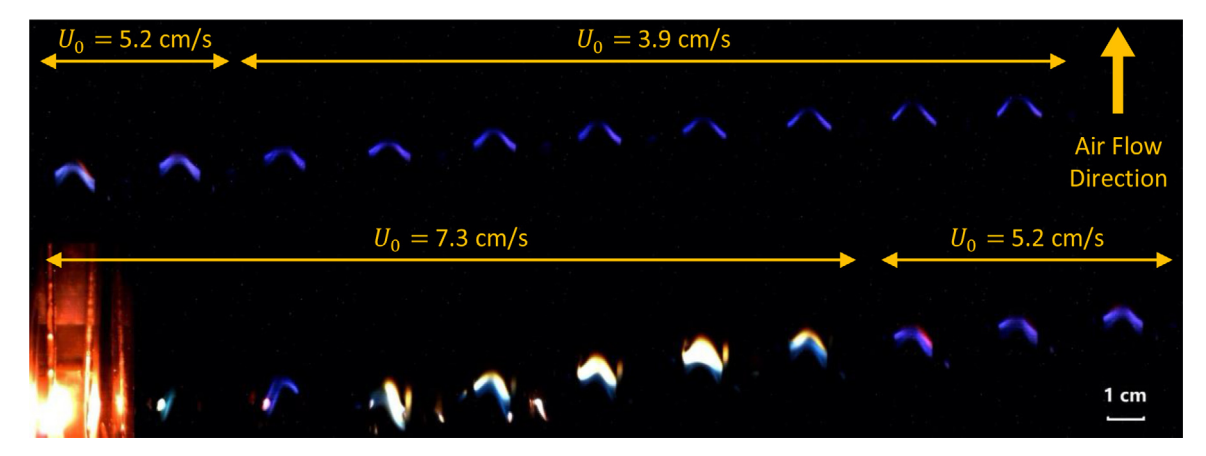


Fig. 9. Transient flame growth of the twin flames (H = 1.0 cm). Ignition is on the lower left and images are 50 s apart, left to right, bottom row to top row.

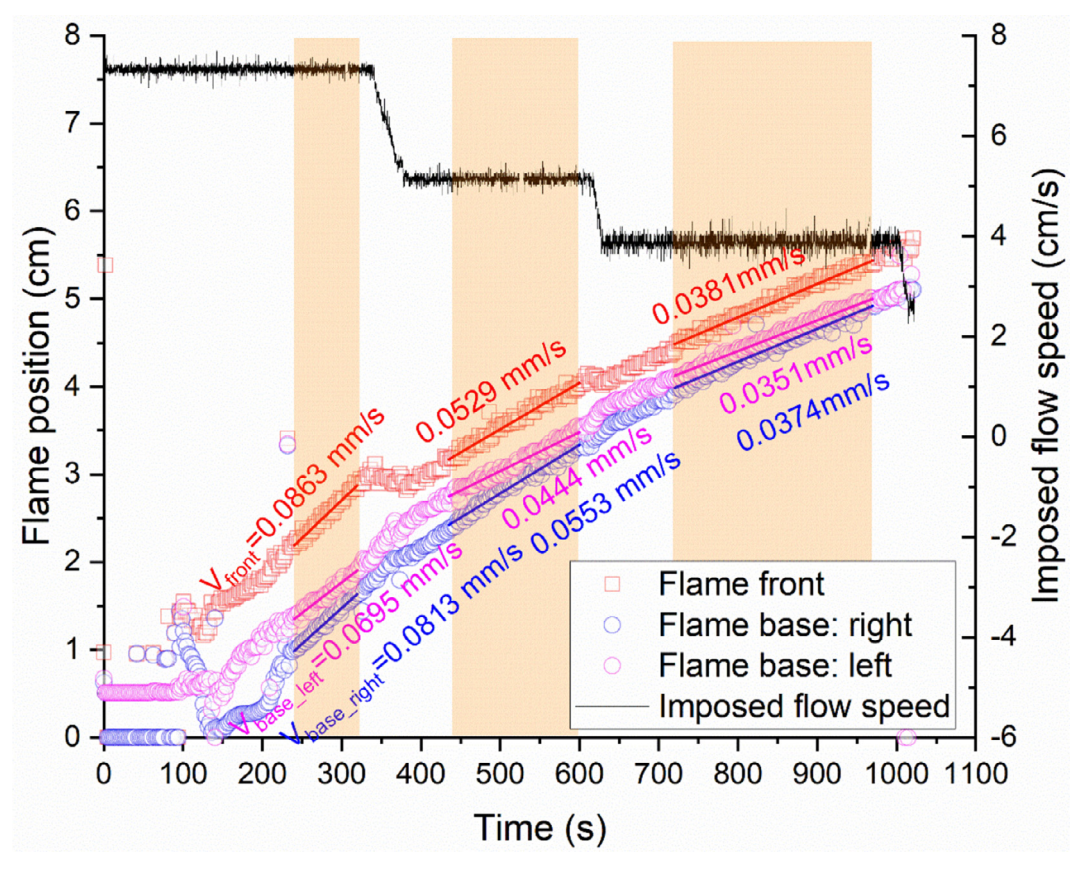


Fig. 10. Flame position and flame length evolution after ignition (twin flames with H = 1.0 cm).

1 cm apart (H=1 cm). One of the samples (the left one in Fig. 9, referred to as the first sample) was ignited using the integrated electric wire (Fig. 2a). As the flame grew and spread downstream, it transferred heat to the second sample through conduction and radiation. At ~ 100 s (Fig. 9, bottom row third image), flame front bent upstream near the second sample, forming an asymmetric " Λ "-shape. This indicates that the second sample, although not yet ignited, reached the pyrolysis temperature and the flame from the first sample consumed the pyrolysates from both samples. As the pyrolysis of the second sample intensified, the right arm of the flame extended further upstream (the base location of the right flame decreases between 100 and 130 s in Fig. 10) and eventually anchored on the surface of the second sample when the sec-

ond sample ignited. The flames from the two samples merged and spread downstream together in a " Λ "-shape.

Notice that initially, the right arm of the twin flames is more upstream due to the delayed ignition of the second sample. While the twin flames propagated downstream, this lagging of the right flame base diminished and the flame shape eventually became symmetric.

It was also observed that in this case, even before the second sample ignited (Fig. 9, bottom row, first three images), the flame is brighter and sootier than single-sided flame with the same flow and confined conditions. This indicates that the parallel sample configuration has a higher flame temperature.

As the imposed flow speed decreases, the flame becomes dimmer and eventually splits in two. When the imposed flow speed

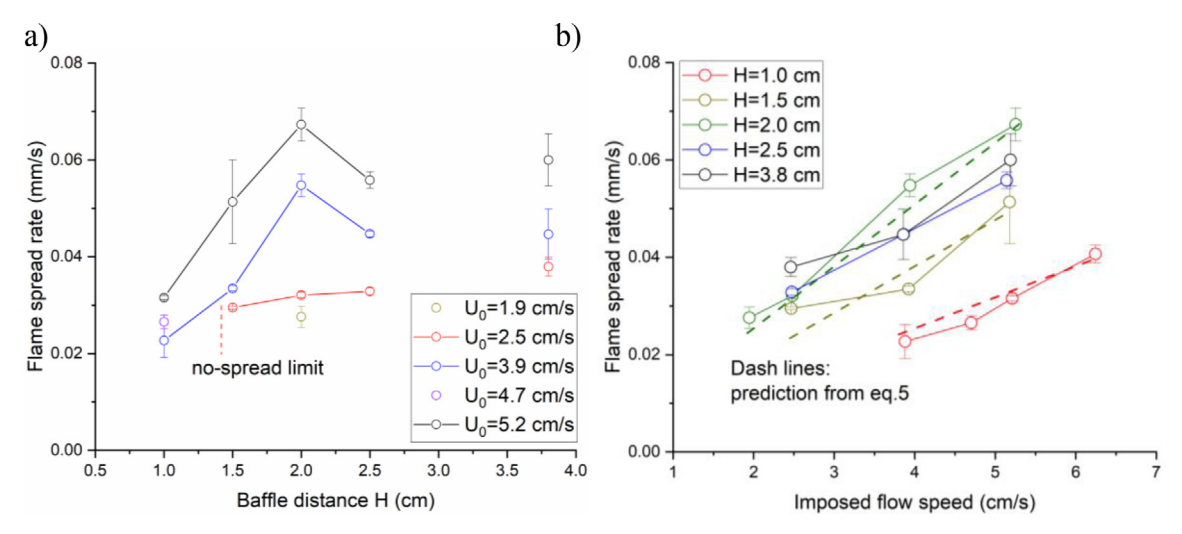


Fig. 11. Single-sided flame spread rates at steady state under different confinement levels and flow conditions. The error bars denote the 95% confidence intervals of the measurements.

decreases further to below 3.9 cm/s, the twin flames quench in a few seconds.

The parallel sample configuration was also tested under confinement $H=1.5\,\mathrm{cm}$. The pyrolysis of the second sample was indicated by occasional sparks near the surface of the second sample. However, the flame was never anchored on the second sample. In other words, the flame from the first sample did not ignite the second sample.

4. Effects of imposed flow speed and confinement

4.1. Flame spread rate and flame length

The steady-state flame spread rates of single-sided flames are compared between different confinement levels and imposed flow speeds in Fig. 11. Similar to previous work [16,22], when the confinement level increases (i.e., H decreases), the spread rate first increases and then decreases. At the same confinement level, the flame spread rate increases with imposed flow speed. While not shown here, the steady state flame length exhibits the same dependencies on the flow speed and confinement level.

Previous research shows that for thermally thin solid fuels in concurrent flows in microgravity, both flame spread rate and flame length at steady state have a linear dependency on the imposed flow speed [4,16,23,24]. This linear dependency remains true for different confined conditions (Fig. 11b). Adjusted flame spread rate and flame length, V_f/U_0 and L_f/U_0 are plotted against baffle distance H in Fig. 12. Data at different flow speeds converges, except for the lowest tested flow speed 2.5 cm/s (when the flame is near quenching).

At H=2.0 cm, the adjusted flame spread rate and flame length are $\sim 25\%$ higher than those at H=2.5 cm. The difference is suspected to be caused by accelerated flows during combustion thermal expansion [16,22,25]. Assuming the volumetric expansion of the hot reacting gas mixture is approximately the same, the flow acceleration is expected to be inversely proportional to the cross-sectional area [16]. As a result, the flame spread rate and flame length are expected to be proportional to 1/H.

For H < 2.0 cm, flame spread rate and flame length are observed approximately linear to the baffle distance. In these confinement levels, combustion is under-ventilated and is controlled by the oxygen supply to the confined space.

Assuming the gaseous fuel production rate equals to the solid degradation rate, the fuel production rate at the steady state can

be expressed as follows.

$$\dot{m}_{fuel} = \tau W_{\rm S} \rho_{\rm S} v_{\rm f} \tag{1}$$

Here, ρ_s , τ , and W_s are the density (1.18 g/cm³), thickness (1 mm), and width (2.2 cm) of the PMMA samples respectively.

The oxygen supply to the combustion zone is approximated as follows.

$$\dot{m}_{O_2} = \rho_{air} U_0 H W_s Y_{O_2} \tag{2}$$

 ρ_{air} is the density of air (1.204 kg/m³ at 20 °C and 1atm) and Y_{O_2} is the mass fraction of oxygen in the air (0.23). When the combustion is under-ventilated and is controlled by the oxygen supplies ($\dot{m}_{fuel}r=\dot{m}_{O_2}$ for complete combustion), flame spread rate can be expressed as follows.

$$V_f = \frac{\rho_{air} Y_{0_2} H}{r \rho_s \tau} U_0 \tag{3}$$

Here, r (= 1.92) is the stochiometric oxygen-fuel mass ratio. Eq. (3) shows that the flame spread rate is proportional to the imposed flow speed U_0 , consistent with the observation shown in Fig. 11b. Eq. (3) also shows that flame spread rate is linearly proportional to the duct height, consistent with Fig. 11a.

In the case with H=3.8 cm (half of the flow duct height), both flame length and spread rate are larger than those at H=2.5 cm. In this case, no baffle is used and the flame is confined between the sample surface and the front window of the flow duct. The front window is made of polycarbonate (Fig. 1b). Compared with the black aluminum baffle, the polycarbonate window has significantly smaller thermal conductivity (0.2 vs. 200 W/m/K) and slightly smaller volumetric heat capacity ($\rho \cdot C_p \sim 1.44$ vs. 2.46 J/cm³/K). Therefore, the flame heat loss to the duct window is expected to be smaller than the heat loss to the baffle. This contributes to a stronger flame at H=3.8 cm.

4.2. Equivalence ratios

The combustion equivalence ratios in all tests are plotted in Fig. 13 based on the following.

$$\phi = \frac{\left(\dot{m}_{fuel}/\dot{m}_{O_2}\right)_{avail}}{\left(\dot{m}_{fuel}/\dot{m}_{O_2}\right)_{stoi}} = \frac{\tau r \rho_s v_f}{\rho_{air} U_0 H Y_{O_2}} \tag{4}$$

As shown in Fig. 13, the equivalence ratio is insensitive to the flow speed. This is because the solid burning rate $(\tau \rho_s v_f W_s \propto U_0)$ and the oxygen supplies to the flame $(\rho_{air} U_0 H Y_{O_2} W_s)$ both increase

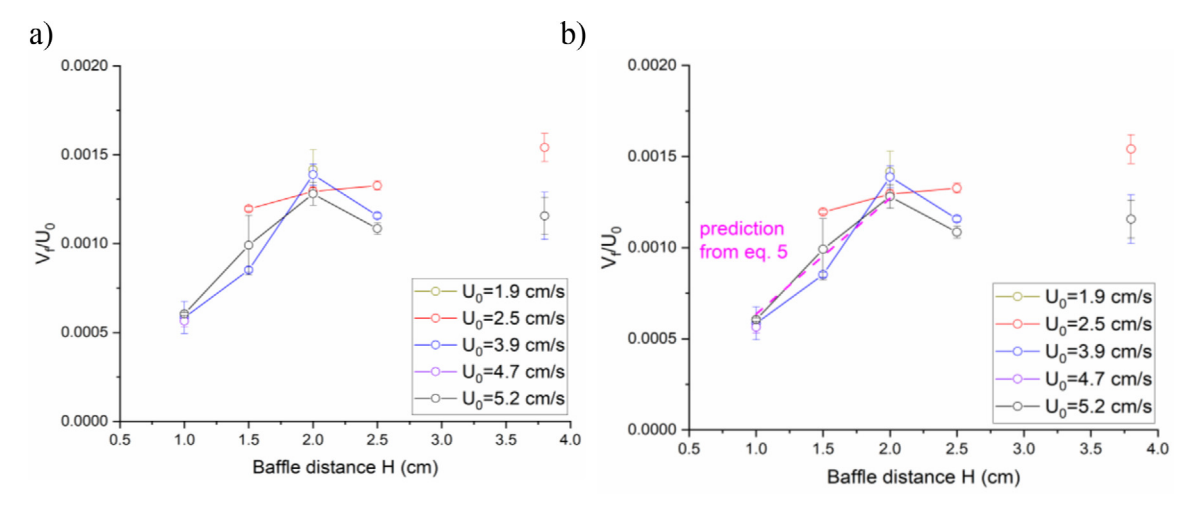


Fig. 12. Single-sided adjusted flame spread rate and flame length at the steady state under different baffle distances.

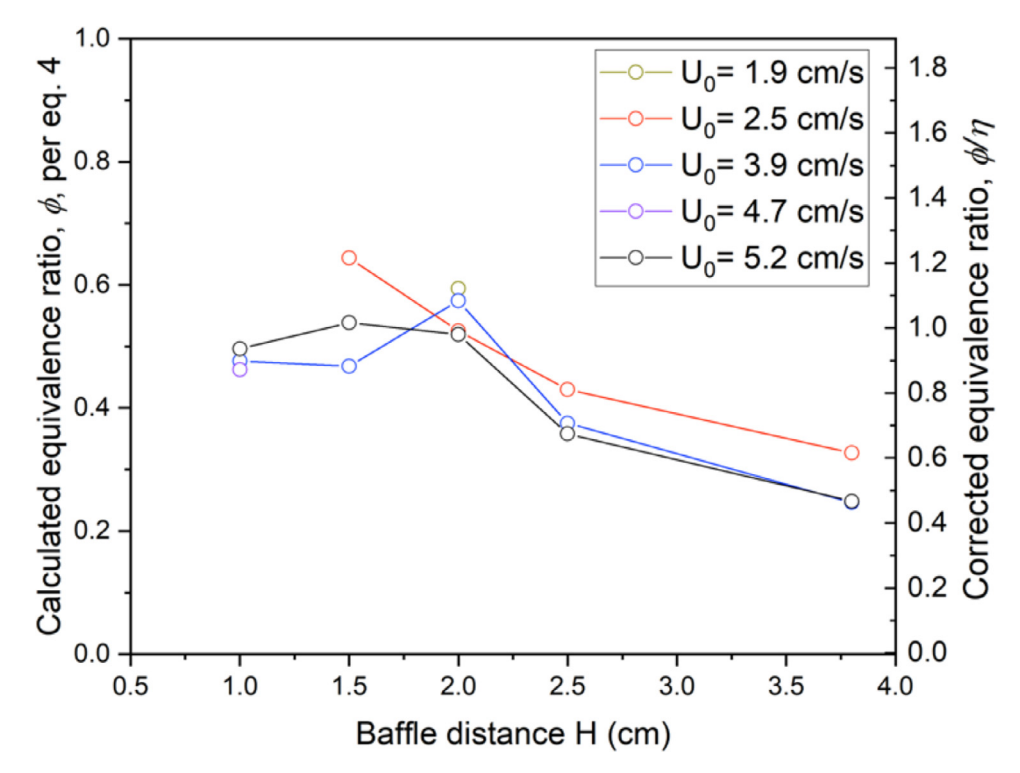


Fig. 13. Combustion equivalence ratio.

with the imposed flow speed. Figure 13 also shows that when H decreases from 3.8 cm to 2.0 cm, the equivalence ratio increases from 0.27 to 0.48. Below the critical baffle distance, the combustion was under-ventilated, and it was expected that the equivalence ratio should be close to unity. However, the calculated equivalence ratios are below unity. In this work, the flame width is similar to the sample width (\sim 2.2 cm) and is significantly smaller than the duct width (7.6 cm). During combustion, flame, through thermal expansion, can act as a pseudo-body [4,24] deflecting incoming flows to the two lateral sides of the combustion zone. This may contribute to the over-estimated oxygen supplies to the combustion zone using Eqs. (2) and (4), resulting in under-estimated equivalence ratios. Nevertheless, Fig. 13 shows that the equivalence ratio remains nearly constant (~ 0.52) when duct height is below the critical duct height. This implies that the combustion is indeed limited by the oxygen supply.

If a correction factor is introduced to the oxygen mass rate in Eq. (2) $(\dot{m}_{O_2,\ corrected} = \eta \dot{m}_{O_2},\ \eta = 0.52)$, the resulting equivalence ratios are shown using the right axis in Fig. 13. Eq. (3) is re-written as follows.

$$V_f = \frac{\eta \rho_{air} Y_{0_2} H}{r \rho_s \tau} U_0 \tag{5}$$

The predicted flame spread rate is plotted in Figs. 12a and 11b. It matches the experimental data reasonably well.

4.3. Heat transfer to sample and baffle surfaces

Flame shapes at steady state are also examined. For each tested condition, ten images, evenly distributed in the flame steady spreading state, are selected and transformed into binary. Averaged pixel values of these binary images and time-averaged flame profiles are then obtained. This procedure filters out disturbance due

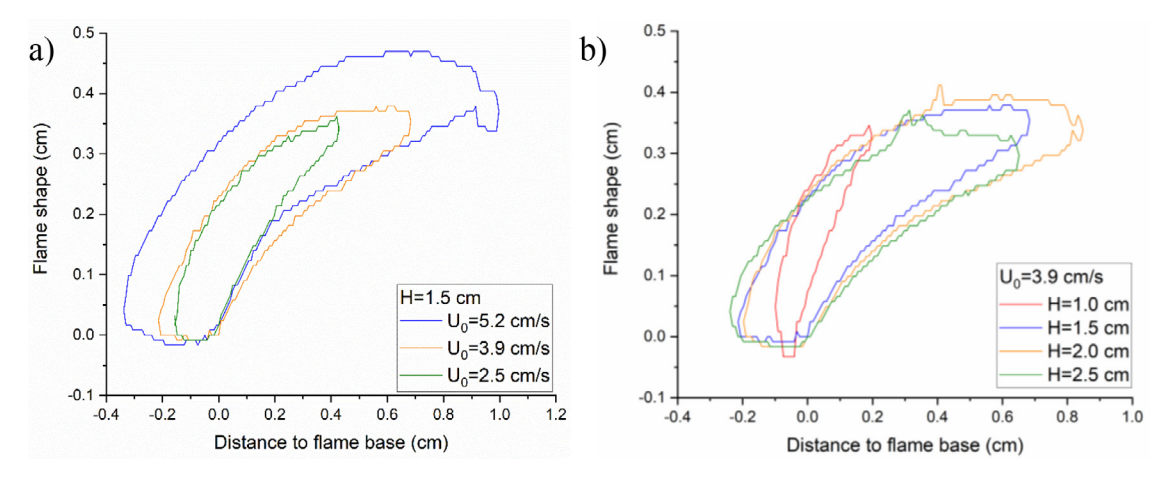


Fig. 14. Flame profiles at different confinement levels and flow speeds.

to fuel vapor jetting and the deduced flame shapes are shown to resemble the flame profile in the raw images. The averaged flame shapes at different flow and confinement conditions are compared in Fig. 14. In general, the flame standoff distance (distance from the flame sheet to the sample surface) is higher in lower flow speeds and in a more confined space (smaller H).

Previous research showed that for flame spread over flat samples, the flame shape resembles the flow viscous boundary layer [24,26]. This is because the fuel pyrolysate needs to diffuse across the boundary layer to meet the oxidizer in the flow stream. As a result, as the flow speed decreases, the boundary layer thickness and the flame standoff distance increase. When the confinement level increases (especially near the quenching limit), oxygen supply to the flame is restricted. A higher flame standoff distance helps increase the oxygen supply to the flame base region.

During the flame spread process, flame transfers heat to the sample and the baffle. Assuming the heat transfer for these small flames is mainly through conduction [27], with approximations of flame sheet and constant flame temperature, the heat transfer rates can be estimated using Fourier's law as follows.

$$q_{sample} = W \int_{0}^{L_f} k_g \frac{T_f - T_p}{y_f} dx$$
 (6)

$$q_{baffle} = W \int_{0}^{L_f} k_g \frac{T_f - T_{amb}}{(H - y_f)} dx$$
 (7)

Here, y_f is the flame standoff distance to the sample surface, deduced from the flame images (Fig. 14), W is the sample width (2.2 cm), and k_g is the conductivity of the air (0.06255 W/m/K, evaluated at film temperature 900 K). T_f , T_p , and T_{amb} are the gaseous flame temperature (1200 K), solid pyrolysis temperature (600 K), and the ambient temperature (300 K) respectively.

Heat of combustion released by the flame is also estimated as follows.

$$q_{comb} = v_f \rho_s \tau W \Delta H_c \tag{8}$$

 $\rho_{\rm S}$ and τ are the density (1.18 g/cm³) and thickness (1 mm) of the PMMA sample respectively. $\Delta H_{\rm C}$ is the heat of combustion (26.81 J/mg) of the PMMA.

The heat of combustion q_{comb} and the heat transfer rates q_{sample} and q_{baffle} are compared between different cases in Fig. 15. Similar to the flame spread rate, heat of combustion and heat transfer to the sample surface exhibit non-monotonic dependency on the baffle distance, H. However, the heat loss to the baffle increases monotonically when the baffle distance decreases. When the baffle is far from the flame, e.g., H > 1.5 cm, the heat loss to the baffle

is negligible compared with the flame heat transfer to the sample surface. When H decreases to 1.0 cm, heat loss becomes comparable to the heat transfer to the sample $(q_{baffle} \sim 65\% \text{ of } q_{sample})$. This increased heat loss to the baffle and the insufficient oxygen supply to the flame eventually lead to a limiting confinement condition for flame spread.

5. Comparisons between different sample configurations

Flame spread rates in the three tested configurations are compared in Fig. 16. At the same confinement level, the double-sided flame has the highest spread rate, followed by the twin flames. For thermally-thin solid fuels, flame spread rate is estimated from the energy conservation in the solid preheat zone as follows [28].

$$v_f = \frac{q'_{pre}}{\rho_s \tau c_{p,s} (T_p - T_0)} \tag{9}$$

Here, $c_{p,s}$ is the specific heat of the solid fuel and q'_{pre} is the net heat input (per unit sample width) to the sample preheat zone.

Assuming the flame heat input to the sample surface is approximately the same for the same confined condition, the double-sided flames are expected to have twice as large of q'_{pre} (the sample is subjected to the flame on both sides) compared to single-sided flames. As a result, the flame spread rate is expected to be twice as large for double-sided flames than single-sided flames (see $H=1.0~{\rm cm}$ in Fig. 16). However, in the experiments, when $H>1~{\rm cm}$, the double-sided flames appeared yellow and sooty even at the minimum tested flow speed (Fig. 7). This is due to strong gas phase reaction and high flame temperatures. The radiation from the soot enhanced the heat input to the sample surface and increased the flame spread rate further. In Fig. 16, when $H>1~{\rm cm}$, flame spread rates for double-sided flames are significantly larger than twice of those for single-sided flames.

When comparing twin flames with single-sided flames, the twin flames should have a higher q'_{pre} due to additional heat input from the second flame. This additional heat input can be approximated as the flame heat loss to the baffle in the single-sided flame configuration. In other words, $q'_{pre,\ TF} = q'_{sample} + q'_{baffle}$ where q'_{sample} and q'_{baffle} are evaluated using Eqs. (6) and 7 respectively.

Figure 15 shows that, at H=1 cm, the baffle heat loss is $\sim 65\%$ of the estimated flame heat transfer to the sample. This explains the $\sim 60\%$ higher spread rate observed for twin flames than single-sided flames in Fig. 16.

As mentioned in Section 3.3, when parallel samples were separated by 1.5 cm, the flame failed to ignite the second fuel. For

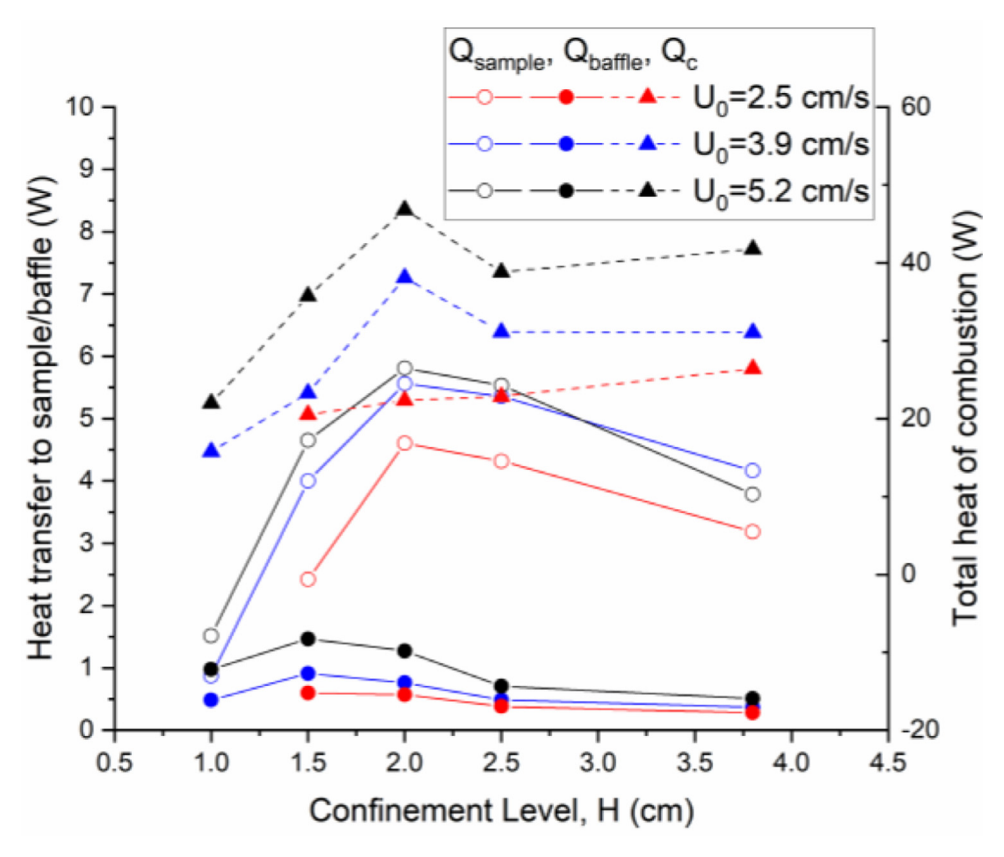


Fig. 15. Estimated combustion heat release and flame heat transfer to the sample and baffle surfaces at different confinement levels.

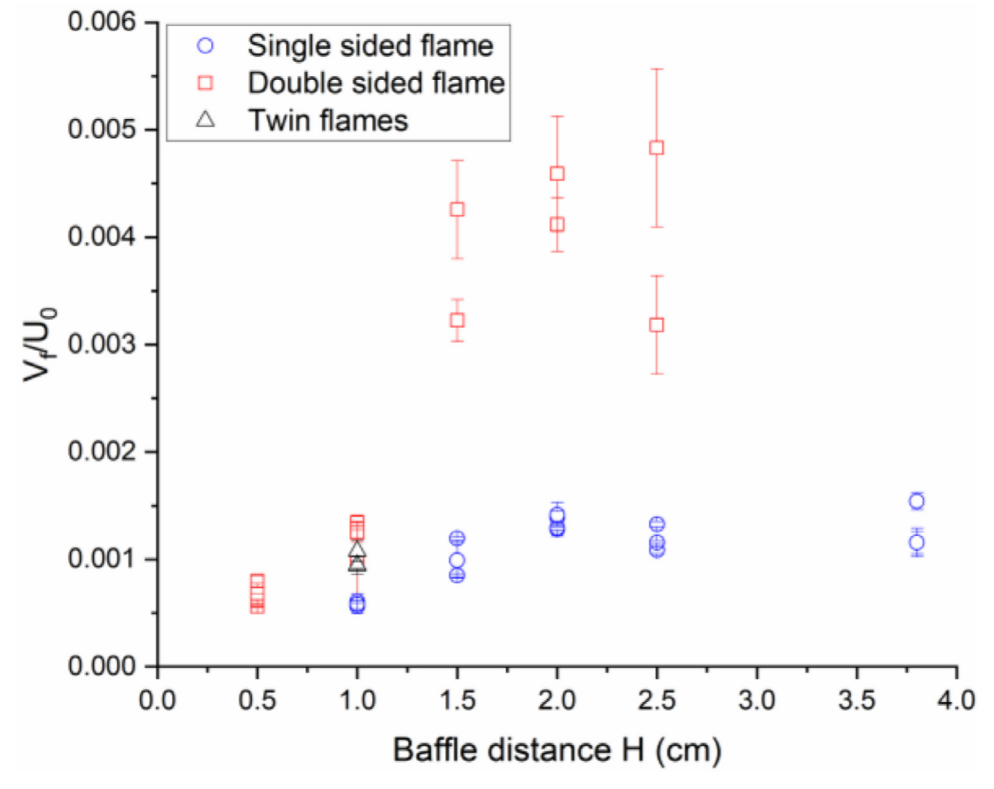


Fig. 16. Adjusted flame spread rates at different sample configurations.

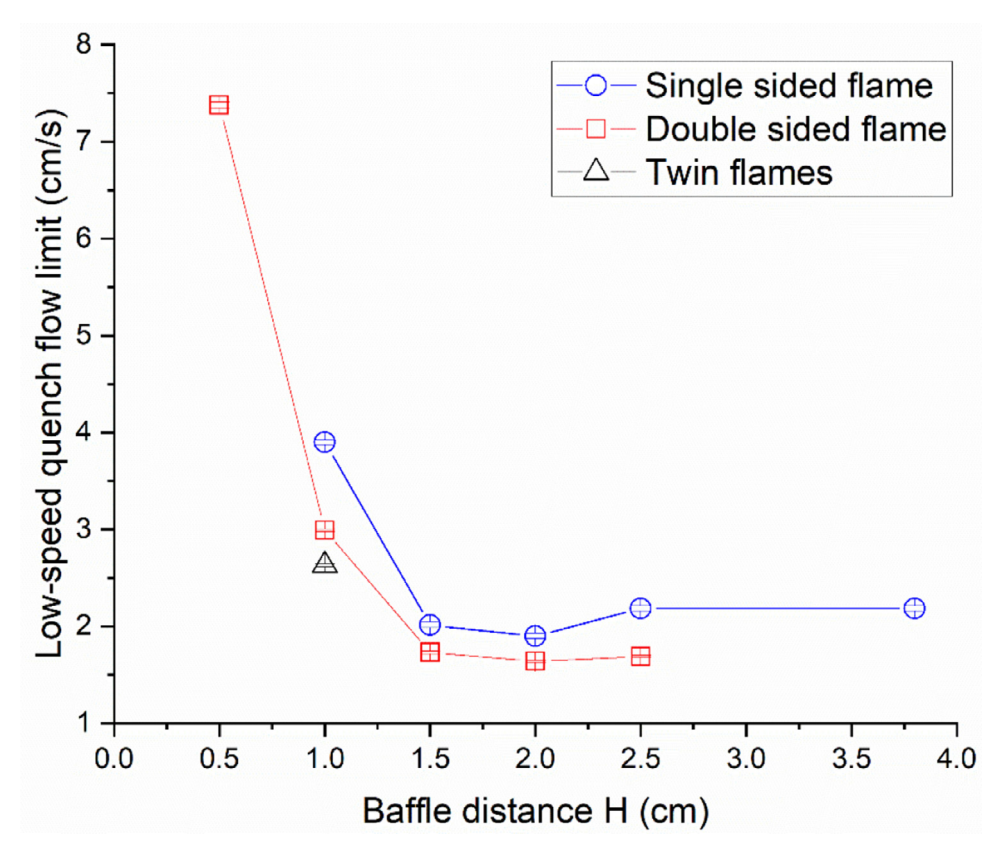


Fig. 17. The no-spread imposed flow speed at different confinement levels and flame types.

solid ignition to occur, a critical heat flux (\sim 10 kW/m² for PMMA [28,29]) is required. The flame heat flux on the second sample is estimated using the single-sided flame profile:

$$q_{sample,second}^{"} = k_g \frac{T_f - T_{amb}}{\left(H - y_f\right)_{min}} \tag{10}$$

When H increases from 1.0 to 1.5 cm, the estimated heat flux reduces to below the critical heat flux for ignition (from 9.9 to 5.5 kW/m^2). The flame failed to ignite the second sample.

The low-speed quenching limits of different configurations are compared in Fig. 17. For both single-sided and double-sided flame configurations, the low-speed quenching limits decrease slightly first and then increase as the baffle distance decreases. The lowest quenching limits are observed at the baffle distance where maximum spread rates occur (H = 2.0 cm). This further indicates that the confinement can increase the flammability of the materials.

At the same confinement level, the twin flame has the lowest quenching limit, followed by double-sided flames. Among the three tested configurations, the twin flame has the highest heat input to the samples and lowest heat loss to the surrounding. This leads to the lowest quenching flow speed. When comparing the double-sided and single-sided flames at the same baffle distance, the double-sided flames have twice as much oxygen supply and heat transfer to solid fuel. These result in a lower quenching flow speed.

6. Remarks

Concurrent-flow flame spread over 1 mm thick PMMA slabs are investigated in a small flow duct aboard the ISS. Three burning scenarios are considered, single-sided, double-sided, and parallel samples. For each burning scenario, confined condition (characterized

by a length scale H) and imposed flow speed are varied and their effects on flame spread are examined. Key findings are as follows.

- 1 For double and single-sided flames, the steady state flame length and spread rate increase first and then decrease when the confinement level increases (or when H decreases) in agreement with [9,14,15,22]. There exists an optimal confinement where the largest flame spread rates, maximum flame lengths, and lowest low-speed quenching limit occur. These indicate that confinement can increase or decrease solid fuel flammability depending on the confined conditions.
- 2 Confinement has multiple effects on the flame. On one hand, it leads to accelerating flow during combustion thermal expansion. This effect intensifies the burning process and enhances the convective heat transfer to solid samples. On the other hand, confinement limits oxygen supply and increases heat loss to surrounding walls. These effects weaken the flame. As a consequence, two flame regimes are observed: ventilation-controlled and kinetics-controlled. When the confinement length scale H is larger than that of the optimal confinement, the flame characteristics are controlled by the accelerated flow and the flame spread rate is inversely proportional to H. When H is smaller than the optimal H, the combustion is limited by the oxygen supply and heat loss. The flame spread rate is proportional to H.
- 3 At each confinement level, flame spread rate and flame length increases linearly with the imposed flow speed.
- 4 At the same confinement level, both double-sided flame and twin flames spread faster and are longer than the single-sided flame. The double-sided flame spread faster because the sample is subject to flame heat input on both sides. The twin flames spread faster because each sample receives additional heat inputs from another flame.

- 5 For parallel samples, when the separation distance H exceeds a certain value, the heat flux from the first burning sample to the second sample drops below the critical heat flux for ignition. The second sample will not be ignited.
- 6 The microgravity experiments provide a rich dataset for model and theory development and validation.

Declaration of Competing Interest

gravity experiments aboard the ISS.

None.

Acknowledgments

This research is co-sponsored by the National Science Foundation and Center for the Advancement of Science in Space (CASIS) under grant number CBET-1740478. Hardware modifications for Confined Combustion and the original BASS hardware were performed by ZIN Technologies. The science team received tremendous support during operations from NASA Glenn Research Center, Marshall Spaceflight Center, and ZIN Technologies (especially from Emily Griffin, Steve Lawn, Russell Valentine, Beth Curtis, Chris Rogers, Wendell Booth), Michael Hall at NASA MSFC, and the Microgravity Science Glovebox team. We would also like to express our immense appreciation to our lab partners in space, ISS crew members Christina Koch, Jessica Meir, Andrew Morgan, Luca Parmitano, Shannon Walker (https://www.nasa.gov/astronauts/biographies/walker-shannon), and Michael Hopkins for supporting and conducting the micro-

References

- K.L. Jamison, D.A. Boardman, A New fire performance test for cavity wall insulation, MATEC Web Conf. 46 (2016) 02004.
- [2] P.V. Ferkul, S.L. Olson, F. Takahashi, M. Endo, M.C. Johnston, J.S. T'ien, Thickness and fuel preheating effects on material flammability in microgravity from the BASS experiment, 29th Annual Meeting of the American Society for Gravitational and Space Research, 2013.
- [3] X. Zhao, Y.-T.T. Liao, M.C. Johnston, J.S. T'ien, P.V. Ferkul, S.L. Olson, Concurrent flame growth, spread, and quenching over composite fabric samples in low speed purely forced flow in microgravity, Proc. Combust. Inst. 36 (2017) 2971–2978
- [4] C. Li, Y.-T.T. Liao, Effects of ambient conditions on concurrent-flow flame spread over a wide thin solid in microgravity, Proc. Combust. Inst. 38 (2021) 4775–4784
- [5] D.L. Urban, P. Ferkul, S. Olson, G. Ruff, J. Easton, J.S. Tien, Y.-T.T. Liao, C. Li, C. Fernandez-Pello, J. Torero, G. Legros, C. Eigenbrod, N. Smirnov, O. Fujita, S. Rouvreau, B. Toth, G. Jomaas, Flame spread: effects of microgravity and scale, Combust. Flame 199 (2019) 168–182.
- [6] B. Comas, A. Carmona, T. Pujol, Experimental study of the channel effect on the flame spread over thin solid fuels, Fire Safety J. 71 (2015) 162–173.
- [7] H. Zhu, Y.G.R. Pan, B. Zhong, Spacing effects on downward flame spread over thin PMMA slabs, Case Stud. Thermal Eng. 13 (2019) 100370.

- [8] H. Zhu, G. Zhu, Y. Gao, G. Zhao, Experimental studies on the effects of spacing on upward flame spread over thin PMMA, Fire Technol. 53 (2017) 673–693.
- [9] H.-.Y. Shih, H.-.C. Wu, An experimental study of upward flame spread and interactions over multiple solid fuels, J. Fire Sci. 26 (2008) 435–453.
- [10] T. Matsuoka, K. Nakashima, T. Yamazaki, Y. Nakamura, Geometrical effects of a narrow channel on flame spread in an opposed flow, Combust. Sci. Technol. 90 (2018) 409–424.
- [11] K. Yasuo, I. Akihiko, C. Mitsuyoshi, Downward flame spread along two vertical, parallel sheets of thin combustible solid, Symp. (Int.) Combust. 17 (1979) 1211–1220.
- [12] S. Hossain, I.S. Wichman, G.W. Sidebotham, S.L. Olson, F.J. Miller, Influence of gap height and flow field on global stoichiometry and heat losses during opposed flow flame spread over thin fuels in simulated microgravity, Combust Flame 193 (2018) 133–144.
- [13] G. Markstein, J.d. Ris, Upward fire spread over textiles, Symp. (Int.) Combust. 14 (1973) 1085–1097.
- [14] S. Wang, J. Hu, Y. Xiao, T. Ren, F. Zhu, Opposed-flow flame spread over solid fuels in microgravity: the effect of confined spaces, Microgravity Sci. Tec. 27 (2015) 329–336.
- [15] S. Olson, J.C. Baukal, Low-Gravity Flames, A Gallery of Combustion and Fire, Cambridge University Press, Cambridge (2020), pp. 74–106.
- [16] Y. Li, Y.-T.T. Liao, P.V. Ferkul, M.C. Johnston, C. Bunnell, Experimental study of concurrent-flow flame spread over thin solids in confined space in microgravity, Combust Flame 227 (2021) 39–51.
- [17] J. Gong, S.I. Stoliarov, L. Shi, J. Li, S. Zhu, Y. Zhou, Z. Wang, Analytical prediction of pyrolysis and ignition time of translucent fuel considering both time-dependent heat flux and in-depth absorption, Fuel 235 (2019) 913–922.
- [18] S.L. Olson, D.L. Urban, G.A. Ruff, P.V. Ferkul, B. Toth, C. Eigenbrod, F. Meyer, Analysis of Saffire II two-sided concurrent flame spread over a thick PMMA slab, 48th International Conference on Environmental Systems, 2018.
- [19] F. Zhu, Z.L.S. Wang, Y. Yin, Microgravity diffusion flame spread over a thick solid in step-changed low-velocity opposed flows, Combust Flame 205 (2019) 55–67
- [20] S.L. Olson, P.V. Ferkul, C. Fernandez-Pello, F.J. Miller, S. Bhattacharjee, I. Wichman, J.S. Tien, Flammability limits from BASS-II testing in microgravity compared to normal gravity limits, 49th International Conference on Environmental Systems, 2019.
- [21] S.L. Olson, P.V. Ferkul, S. Bhattacharjee, F.J. Miller, J.S. Tien, I. Wichman, Results from on-board CSA-CP and CDM sensor readings, 45th International Conference on Environmental Systems, 2015.
- [22] Y. Li, Y.-T.T. Liao, P. Ferkul, Numerical study of the effects of confinement on concurrent-flow flame spread in microgravity, J. Heat Transf 142 (2020) 11301.
- [23] S.L. Olson, F.J. Miller, Experimental comparison of opposed and concurrent flame spread in a forced convective microgravity environment, Proc. Combust. Inst. 32 (2009) 2445–2452.
- [24] A. Vetturini, W. Cui, Y.-T. Liao, S. Olson, P. Ferkul, Flame spread over ultrathin solids: effect of area density and concurrent-opposed spread reversal phenomenon, Fire Technol. 56 (2020) 91–111.
- [25] Y. Li, Y. Liao, P. Ferkul, Concurrent-flow flame spread over a thin solid in a narrow confined space in microgravity, 2019 International Mechanical Engineering Congress & Exposition, 2019.
- [26] A. Carney, Y. Li, Y.-T. Liao, S. Olson, P. Ferkul, Concurrent-flow flame spread over thin discrete fuels in microgravity, Combust Flame 226 (2021) 211–221.
- [27] A.C. Fernandez-Pello, Flame spread in a forward forced flow, Combust Flame 36 (1979) 63–78.
- [28] J.G. Quintiere, Fundamentals of Fire Phenomena, John Wiley & Sons Ltd, West Sussex, England (2006), pp. 172–175.
- [29] V. Babrauskas, Ignition Handbook: Principles and Applications to Fire Safety Engineering, Fire Investigation, Risk Management and Forensic Science, Fire Science, Issaquah, WA, 2003.